Surface reconstruction of FeAl(110) studied by scanning tunnelling microscopy and angle-resolved photoemission spectroscopy

2004 J. Phys.: Condens. Matter 16 5395

(http://iopscience.iop.org/0953-8984/16/30/002)

INSTITUTE OF PHYSICS PUBLISHING JOURNAL OF PHYSICS: CONDENSED MATTER

J. Phys.: Condens. Matter **16** (2004) 5395–5406 PII: S0953-8984(04)81652-7

Surface reconstruction of FeAl(110) studied by scanning tunnelling microscopy and angle-resolved photoemission spectroscopy

O Kizilkaya[1,2], D A Hite[3], D M Zehner[4] and P T Sprunger[1,2,5]

[1] Center for Advanced Microstructures and Devices, Louisiana State University, Baton Rouge, LA 70806, USA
[2] Department of Physics and Astronomy, Louisiana State University, Baton Rouge, LA 70803, USA
[3] Electromagnetics Division, National Institute of Standards and Technology, Boulder, CO 80305, USA
[4] Condensed Matter Sciences Division, Oak Ridge National Laboratory, Oak Ridge, TN 37831, USA

E-mail: phils@lsu.edu (P T Sprunger)

Received 2 June 2004
Published 16 July 2004
Online at stacks.iop.org/JPhysCM/16/5395
doi:10.1088/0953-8984/16/30/002

Abstract

The surface geometric and electronic structure of the FeAl(110) intermetallic alloy has been investigated by scanning tunnelling microscopy and angle-resolved photoemission spectroscopy (ARPES). Preferential sputtering results in depletion of Al in the surface region and subsequent annealing promotes surface segregation of Al and gives rise to new reconstructed phases. A bulk terminated surface structure is obtained after annealing the surface to 400 °C. However, an incommensurate phase develops above 800 °C with a stoichiometry consistent with an $FeAl_2$ structure in the topmost layer. The ARPES measurements confirm the Al segregation with increased density of states (DOS) near the Fermi level. The increased DOS is believed to be due to hybridization between the Fe d and Al sp states. The increased intensity of the Al 2p core level for the incommensurate phase also confirms the higher Al surface concentration for this phase.

1. Introduction

The fundamental importance of intermetallic alloy surfaces lies in their impact on corrosion resistance, oxidation, catalytic activity, and electrochemistry [1, 2]. The physical and chemical properties of the intermetallic alloy in these applications are determined by the structure and

[5] Author to whom any correspondence should be addressed.

composition of the surface and near surface layers. Small alterations to the structure and the composition of the intermetallic alloy surface may drastically enhance or diminish these properties. In order to predict and modify these properties, a detailed understanding of the *surface* atomic and electronic structure of metal alloys is required.

Surface segregation is one of the foremost mechanisms that change the surface composition by enrichment of one component in a binary alloy's surface region. In contrast to the case for a random alloy wherein one of the alloy constituents segregates to the surface selvage region, ordered intermetallic alloys do not favour segregation due to their strongly attractive chemical bonding between the constituents of the alloy. Surface segregation is inhibited by these interactions and surfaces are typically terminated with a bulk stoichiometric composition.

The late transition metal alloys, for example NiAl and FeAl, have received much attention due to their technologically attractive and unique properties, such as high melting points, enhanced corrosion resistance, relatively low density, and utility as soft magnetic materials. In contrast to the local bonding for early transition metal alloys, e.g., TiAl and VAl, which are dominated by a strong directional interaction between the nearest transition metal neighbours, in the late transition metal alloys a significant charge transfer and resultant hybridization occur between the Al sp and transition metal d states which dictate the overall bonding and ensuing properties [3].

The late transition metal alloys crystallize in a CsCl-type structure effectively forming a bcc lattice. The close packed (110) surfaces of NiAl and CoAl exhibit bulk terminated structures. The higher melting points and higher heat of formation of these alloys make them very stable at room temperature. Remarkably, both low energy electron diffraction (LEED) intensity–voltage data and medium energy ion scattering data have revealed an in-plane, rippled relaxation as Al atoms are displaced out of the surface by 0.02 nm and Ni atoms are contracted towards the bulk by 0.012 nm with respect to their bulk position [4, 5]. The CoAl(110) surface also exhibits surface rippling as the Al plane of atoms protrudes 0.018 nm with respect to Co plane of atoms [6]. Most notably however, previous LEED and Auger electron spectroscopy (AES) studies by Graupner *et al* [7, 8] revealed that FeAl(110) does not follow the trend of NiAl(110) and CoAl(110).

These latter studies reported that the clean surface of FeAl(110) does not exhibit the structure and composition of the bulk truncated surface. As in other transition metal alloys, ion sputtering is employed to clean the surface, and this process results in a depletion of Al in the selvage region. Unlike the other intermetallic alloy surfaces, sequential annealing of the Al depleted FeAl(110) surface does not restore the surface to its bulk stoichiometry. In fact, the annealing promotes an enhanced Al segregation to the surface and consequently leads to surface reconstruction and development of different atomic structures, or superstructures, in the surface region as a function of annealing temperature. Whereas LEED reveals a (2×1) structure upon annealing the surface to 400 °C, an incommensurate superstructure develops in the temperature ranges 400–600 °C and above 800 °C [7]. For annealing in the temperature range of 600–800 °C, severe streaking occurs in the LEED patterns along the $[1\bar{1}0]$ direction of the substrate. Surprisingly, no (1×1) diffraction pattern, which corresponds to a bulk terminated (110) surface, was observed with LEED over the entire annealing temperature range. This result [7, 8] is in contrast to that of an earlier LEED study by Gleason *et al* wherein a bulk terminated surface of FeAl(110) was reported based on a (1×1) diffraction pattern [9].

The characterization of surface atomic and electronic structure is vital for nanoengineering the physical and chemical properties of alloys and their resultant applications. However, the previous studies of Graupner *et al* give only a qualitative picture of the surface of FeAl(110). In the present study, we extend the elucidation of this unique surface's properties with two

invaluable surface probes, STM and ARPES, which help to yield a correspondence between the local atomic and electronic structure of the annealing temperature dependent phases at the surface.

We will present and discuss the atomic and electronic structure of the FeAl(110) surface for two distinct phases. The first is formed upon annealing to a temperature of 400 °C, wherein the atomic and electronic data astonishingly reveal a bulk terminated surface. This phase is compared and contrasted with the phase that is formed upon annealing to temperatures above 800 °C. This latter phase, which is the lowest energy configuration for this surface, forms a reconstructed phase with a stoichiometry consistent with $FeAl_2$. The structures of phases between these temperature ranges show disordered surfaces and are detailed in a forthcoming article [10].

2. Experimental details

The FeAl single crystal was grown at the Max-Planck-Institut für Eisenforschung in Germany. The lattice constant was determined with x-ray diffraction as $a = 0.2903$ nm corresponding to a constituency of $Fe_{0.53}Al_{0.47}$ [11]. This composition of the constituents prevents the phase transition between FeAl and $FeAl_2$ structures at low temperatures [12]. The sample was cut by spark erosion and aligned to $\pm 0.3°$ using Laue diffraction. The (110) oriented surface was mechanically polished using carborundum followed by 1 μm alumina powder. The sample was mounted on a Ta sample platen with a K-type thermocouple attached to determine the sample temperature for the STM study. For the ARPES measurements, the sample was placed on a 2 cm^2 Ta sheet with two W wires passed through the sides of the crystal for resistive heating. The substrate was cleaned by repeated cycles of sputtering at room temperature (Ne^+ ions, 1 keV, 20 μA). The surface cleanliness was confirmed by the sharp LEED diffraction spots and photoemission spectra of the clean FeAl(110) surface.

Preliminary STM experiments were carried out at Oak Ridge National Laboratory, employing an Omicron room temperature Scanning Probe Microscope. Additional STM experiments were performed using a variable temperature STM at Louisiana State University. Both measurements were conducted in ultrahigh vacuum surface science chambers, equipped with LEED, a cylindrical mirror analyser, and a quadrupole mass spectrometer. Atomic resolution could be obtained on a routine basis with these microscopes.

The ARPES data were obtained at the Center for Advanced Microstructures and Devices, using the six-metre toroidal grating monochromator (6m-TGM) beamline. The normal emission measurements were taken with s + p polarized light at a 45° incident angle. The FeAl(110) crystal was rotated in the plane of incidence for ARPES dispersion measurements since the 6m-TGM beamline analyser, VSW HA150, is fixed.

3. Results and discussion

3.1. Atomic structure of FeAl(110)

The driving mechanism for the large rippled relaxation in the NiAl(110) surface has been studied in several theoretical papers and is related to charge distribution in the surface region, which is different from that in the bulk [4]. The modified charge distribution has a large impact on the relaxation mechanism; specifically, the Al atoms move towards the vacuum region to allocate more space for the compressed sp electrons. Ni atoms, which possess strongly localized d electrons, are contracted inward due to the electrostatic interaction with the redistributed sp electrons. The relaxation is smaller in the deeper layers compared to the

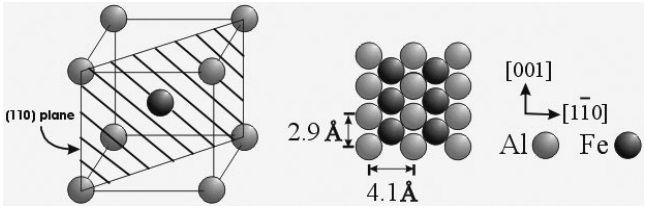

Figure 1. The models illustrate the (110) plane of the bcc lattice of FeAl crystal.

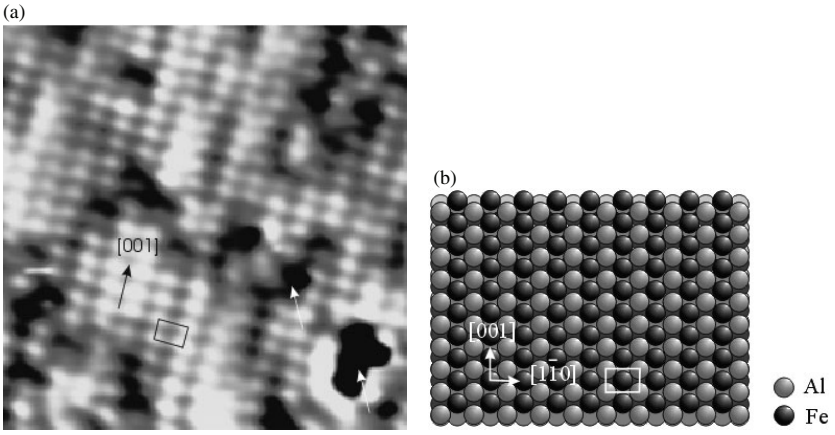

Figure 2. (a) An STM image (4.7×4.7 nm^2, $I_t = 3.96$ nA, $V_t = 331$ mV) of the bulk terminated surface and (b) the ball model.

topmost layer and the bulk arrangement is restored within a few layers. Like NiAl, FeAl crystallizes in the CsCl structure, which has two interpenetrating simple cubic sublattices of Fe and Al. Its bulk terminated (110) surface consists of the composite layers of Al and Fe parallel to the surface. As shown in figure 1, the chains of Fe and Al alternate and are coplanar. As for the experimental results for NiAl(110), a bulk terminated surface is naively expected; however, the truncated bulk (110) surface was absent in previous AES and LEED studies [7, 8].

The Al depleted surface produced due to preferential sputtering gives rise to several superstructures upon sequential annealing. With the estimated depth of 0.42 nm for Auger electrons, an $Fe_{59}Al_{41}$ stoichiometry was calculated in the near surface region. Annealing the Al depleted surface to 400 °C results in diffusion of Al from the bulk to the surface region and forms a (2×1) superstructure [7]. Previous structural studies [8] suggested that this surface structure results from the metastable formation of a subsurface slab of Fe_3Al, similar to that of FeAl(100) that develops in this temperature region. The FeAl(100) surface is capped with an Al layer and the surface Al atomic concentration was calculated to be 0.32 [13]. This result agrees well with the bulk phase diagram wherein a Fe_3Al structure is thermodynamically stable at 400 °C. As detailed below, our STM and ARPES results for this annealing temperature rule out the proposed subsurface Fe_3Al structure for FeAl(110).

The atomically resolved STM image in figure 2(a) is obtained after annealing the sample to 400 °C. The unit cell drawn with a solid line in the figure matches the unit cell of the bulk terminated FeAl(110) surface as depicted in the ball model in figure 2(b). In addition to STM and ARPES data (detailed below), a (1×1) pattern in LEED (not shown) confirms that the surface structure is a truncated bulk (110) surface at this temperature. Although

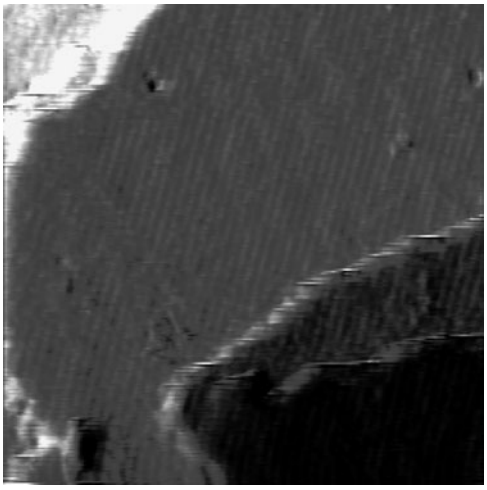

Figure 3. An STM image of a (15×15 nm^2, $I_t = 1.83$ nA, $V_t = 954$ mV) bulk terminated FeAl(110) surface, revealing relatively defect-free atomic terraces.

overall a (1×1) structure is revealed (see the unit cell grid in figure 2(a)), STM images indicate that the surface also contains vacancy-type defect sites as shown with arrows in figure 2(a). It is believed that, due to kinetic effects in the segregation process, defects reflect regions of locally low Al concentration (below 50%). This tentative assessment is based on the number of observations. Previous AES/LEED studies on FeAl(110) [7, 8] reported that there is only a narrow temperature range (∼360–410 °C) wherein the Al concentration is ∼0.5 and a (2×1) LEED pattern is observed. This strongly suggests that kinetic factors are dictating the composition and structure in the near surface region in this temperature region. In the present case, only a (1×1) LEED pattern is observed which thus indicates that the composition at a given temperature may not be exactly equivalent to that in the previous study. Knowing that the Al surface concentration is rapidly increasing around 400 °C due to bulk segregation, the observed depressions in the STM image are interpreted as being Al vacancies, which decreases the surface order.

However, larger scale images (15×15 nm^2; figure 3) indicate that the overall morphology of the surface is quite flat with relatively large atomic terraces. This indicates that, in spite of the local Al vacancy defects, the well-ordered surface structure can be characterized as bulk terminated FeAl(110). STM images clearly indicate that the surface does not exhibit any inhomogeneity or the formation of an incommensurate structure (e.g., a Fe_3Al subsurface slab), as proposed in previous studies [14].

A closer comparison between the unit cells highlighted in the atomically resolved STM image and in the ball model (figures 2(a) and (b)) indicates an apparent inconsistency. Specifically, it appears as if only one of the two atoms per unit cell is clearly visible in the STM image. Although STM elucidates surface morphology in real space with atomic resolution, it does not reveal the chemical contrast between the different atom species for alloy surfaces, provided that no large differences in atom sizes exist. In view of this, the chemical identity of the atoms in figures 2(a) and 3 could not be *directly* determined. However, with assumptions on the tunnelling process and knowledge of the surface electronic structure, one can infer the chemical speciation of the binary alloy surface. Although ARPES results, detailed below, show that the local density of states (LDOS) near E_F is dominated by Fe 3d states, one may

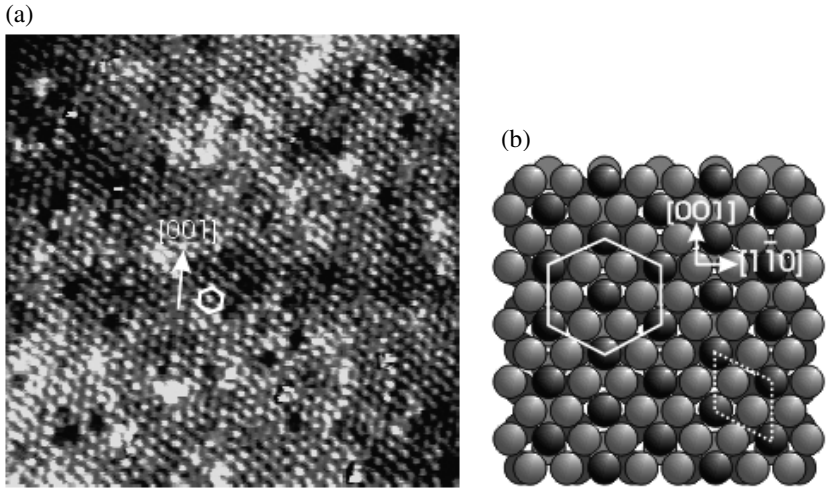

Figure 4. (a) An STM image (15×15 nm^2, $I_t = 5.41$ nA, $V_t = 30.2$ mV) of an FeAl(110) surface after annealing to 850 °C. (b) A ball model displaying Fe atoms surrounded by six Al atoms and a unit cell of $FeAl_2$ stoichiometry.

then interpret the periodic atomic protrusion structure indicated in figure 2(a) as due to Fe atoms. However, Fe d states are quite localized and they rapidly decay away from the sample surface. In addition, Al sp states exhibit a delocalized nature and hence contribute primarily to the tunnelling mechanism and the apparent protrusion structure as viewed with STM. This assessment has been confirmed through a theoretical investigation of NiAl(110) [15] wherein the simulated STM image generated by Tersoff–Hamann theory shows that the imaged atoms are indeed the Al atoms at the surface. In the present study we also assume that Al atoms dominate the STM image. That is, comparing the STM image with the ball model in figure 2(b), the Fe atoms at the centre of the rectangular Al array are apparently absent.

In the temperature range of 400–600 °C, an incommensurate structure is observed due to higher Al segregation (i.e., >0.5) to the near surface region. STM reveals that this structure does not have long range order. In the range of annealing temperature 600–800 °C, the superstructure diffraction pattern for the incommensurate structure is replaced by severe streaking on the LEED pattern. Strong streaking along the $[1\bar{1}0]$ direction indicates a disordered structure along this direction. Both of these intermediate temperature phases [10] are metastable phases.

Finally, a surface structural transition from this 'streaking' phase to an incommensurate phase takes place at temperatures above 800 °C. On the basis of our experimental results, it is believed that this is the lowest energy configuration. Our LEED pattern from this phase is consistent with prior studies [7, 8]. Moreover, these previous studies indicate that the Al concentration in the near surface region c_{Al} is 0.58 with the concentration relation $c_{Al} + c_{Fe} = 1$ for this phase [7]. Assuming the enhanced segregation Al atoms are confined to the topmost layer, the topmost concentration of Al turns out to be 0.67 ± 0.06, corresponding to $FeAl_2$ stoichiometry within the topmost atomic layer. In close agreement with this assessment, which was based on AES data, a more recent x-ray diffraction (XRD) experiment confirms a $Fe_{0.35}Al_{0.65}$ stoichiometry for this phase [16] where correspondingly a structural model of this incommensurate surface $FeAl_2$ phase has been proposed.

The STM image in figure 4(a) reveals the detailed atomic structure of this incommensurate phase. Variation in the tunnelling parameters did not significantly alter the observed structure.

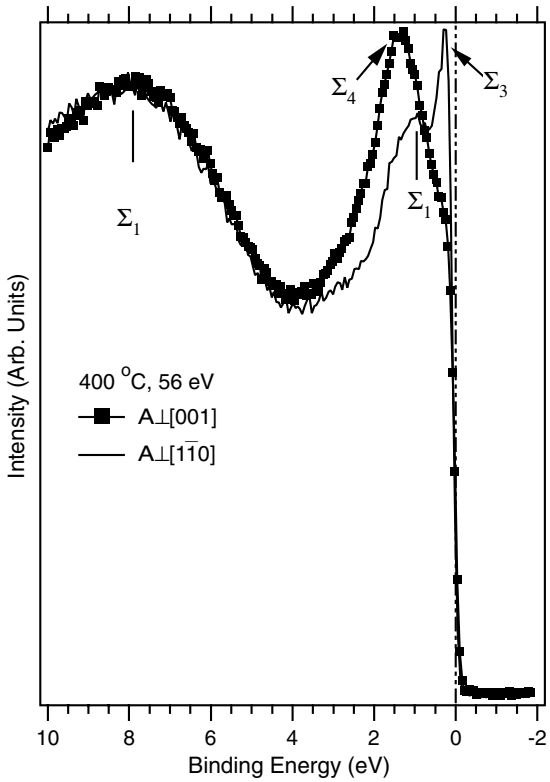

Figure 5. EDCs of clean FeAl(110) after annealing to 400 °C for both symmetry directions of the FeAl(110). The normal emission and 45° incident angle are used.

The image shows an atomically resolved quasi-hexagonal arrangement of atoms. The structural model, seen in figure 4(b), determined from the STM image agrees well with the previous LEED and XRD studies of the incommensurate phase structure [8, 16]. The unit mesh, shown with a dashed line, encompasses one Fe and two Al surface atoms. Comparing the STM data and the ball model, the hexagon mesh drawn with a solid line (figure 4(b)) is now consistent with the imaged atoms being Fe, surrounded by six Al atoms, which are not imaged with STM. The strong agreement with STM, XRD and LEED findings confirms the proposed surface $FeAl_2$ structure and correspondingly indicates a bulk stoichiometry for the subsurface. Regarding the proposition that the hexagonal arrangement observed with STM corresponds to the Fe atoms, the model developed from the previous x-ray reflectivity includes a local outward surface relaxation of the Fe atoms. That is, our assessment that the Fe atoms protrude normal to the surface plane is consistent with the XRD study. In addition, the STM measurements indicate that due to the periodicity along the [001] direction, 0.42 nm, as compared to the periodicity of the underlying substrate, 0.29 nm, it lacks commensurability along this particular direction. However, the distance between two successive Fe atoms is measured as 0.822 nm in the [1$\bar{1}$0] direction of the substrate. This indicates that this phase is commensurate with the underlying substrate only along this direction.

3.2. Electronic structure of FeAl(110)

For late transition metal alloys, as the Al concentration increases in the alloy, the charge transfer from Al to the transition metal also increases. This phenomenon affects the hybridization

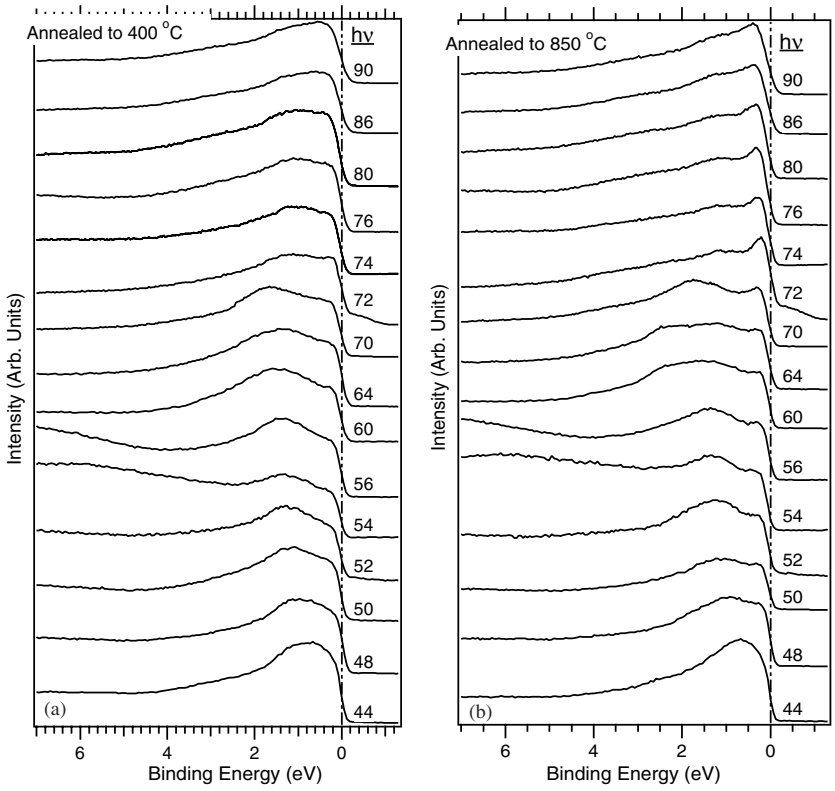

Figure 6. EDCs of (a) bulk terminated and (b) incommensurate clean surfaces collected at normal emission and within the geometry with $\vec{A} \perp [001]$.

between Al sp and transition metal d states and changes the interaction between the states, which in turn affects the chemical and physical properties of the transition metal alloy. It was reported by Kang and Mele that the redistribution of sp electrons around the Al atoms in the topmost layer of NiAl(110) and the localized surface states dictates the surface rippling [17].

In the present study, the surface/bulk band structure of FeAl(110) has been investigated with ARPES utilizing synchrotron radiation. For normal emission measurements, the states having Σ symmetry along the ΓM symmetry line are probed. The density of states and band structure of FeAl(110) have been calculated by Das *et al* using the self-consistent scalar relativistic tight-binding method in the atomic sphere approximation [18]. The calculated band structure reveals that the bands from the Fermi level to 2.75 eV are dominated by Fe d bands and the Σ_1 band, centred on 8 eV, has an s-like characteristic. Along the Σ symmetry line, the allowed dipole transitions are from Σ_1, Σ_3, and Σ_4 symmetry; transitions from the Σ_2 initial state are forbidden by symmetry in normal emission measurements. It is well acknowledged that implementing the polarization of light and the symmetry of the crystal gives rise to the identity of the initial state. With s polarized light, Σ_3 and Σ_4 states are excited with the vector potential ($\vec{A}$) along the [001] and [1$\bar{1}$0] directions, respectively. Σ_1 is identified with p polarized light in both mirror planes of FeAl(110).

The energy distribution curves (EDCs) in the present study were collected with normal emission and a 45° incident angle, corresponding to s + p polarization. The EDCs displayed in figure 5 were acquired after annealing the clean surface to 400 °C, wherein the surface exhibits the bulk terminated surface detailed above. A photon energy of 56 eV was used and two

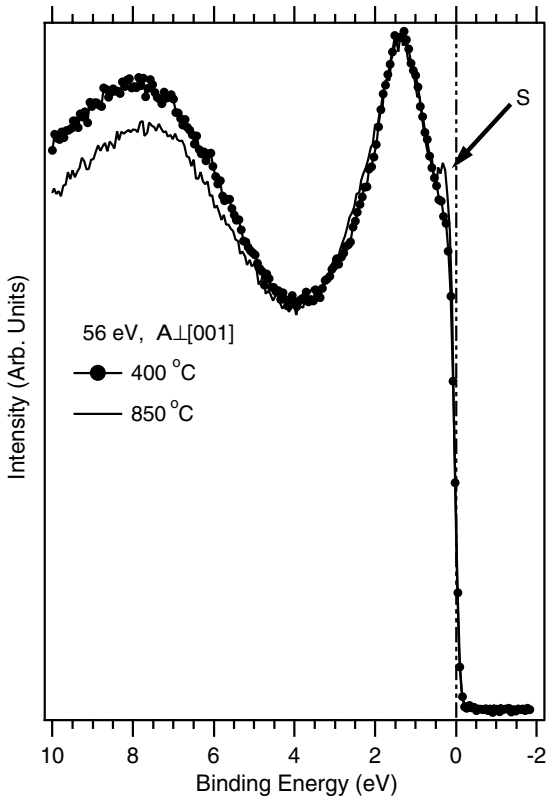

Figure 7. EDCs of clean FeAl(110) for bulk terminated and incommensurate surfaces collected at normal emission and for $\vec{A} \perp [001]$ geometry. The incommensurate phase exhibits a Σ_3 derived new state labelled S.

symmetry geometries are employed by aligning the vector potential along either the [001] or the $[1\bar{1}0]$ direction of the FeAl(110) surface, via *in situ* rotation of the crystal about its normal. Comparing these states with the calculated bulk bands [18] and applying the dipole selection rules, the identity and symmetry of the bands in figure 5 are easily determined. The shoulder at 1.5 eV and broad peak at 8 eV are identified as corresponding to a Σ_1 state. The peak at 0.2 eV is characterized as corresponding to a Σ_3 state, which is an allowed transition with the vector potential, $\vec{A}$, parallel to the [001] direction. The peak that appears at 1.8 eV is identified as corresponding to a Σ_4 state, which is a dipole allowed state in the $\vec{A} \perp [001]$ geometry. These results indicate that the states near the Fermi edge are dominated by Fe d states and they show very good agreement with the calculated band structure, implementing a free electron final state for a photon energy of 56 eV.

To elucidate the impact of segregation on the valence band structure and symmetry, we measured EDCs at room temperature after annealing the sample to 400 °C, where the surface structure is bulk terminated (1×1), and 850 °C, where an incommensurate surface $FeAl_2$ phase forms. EDCs taken in normal emission geometry (i.e., perpendicular momenta with Σ symmetry) as a function of incident photon energy reveal the energy dispersion of the valence bands. Figures 6(a) and (b) show the normal emission EDCs for the bulk terminated and incommensurate phases, respectively. The only major difference between these two spectra is the increased DOS near the Fermi edge for the incommensurate phase compared to bulk

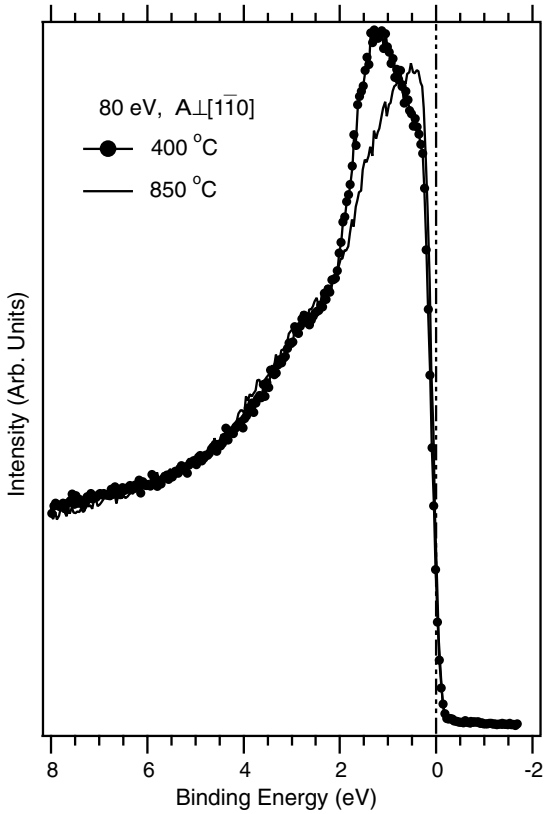

Figure 8. EDCs of clean FeAl(110) for bulk terminated and incommensurate surfaces collected at normal emission and for $\vec{A} \perp [1\bar{1}0]$ geometry.

terminated surface. The EDCs show similar dispersions along the ΓM direction for the two surfaces. At a photon energy of 56 eV, the electronic structure elucidated by ARPES is effectively a combination of surface and near surface. Thus, the strong similarity between the valence structures of the two structural phases indicates similar atomic structure. Although somewhat indirect, this experimental observation adds further support to the notion that the underlying surface slabs for two surfaces have nearly the same composition and structure. On the basis of our STM, ARPES, and LEED findings, a model that includes a subsurface Fe_3Al slab can be excluded. Our results are consistent with a near bulk-like structure in the subsurface region and only the surface differs in structure/composition as a function of annealing temperature.

Since the increased Al concentration at elevated temperatures will reduce the surface symmetry and modify the surface potential, it is expected that the interaction between the Fe d states and Al sp states will increase the hybridization between these states. The EDCs for the bulk terminated surface and incommensurate surface, taken at 56 eV photon energy with normal emission geometry, are displayed in figure 7. The only major difference between the valence structures of these two phases is a new feature, labelled S, which appears near the Fermi level (∼0.3 eV) in the incommensurate phase spectrum. Energetically, this state emerges at the same energy as the theoretically predicted Σ_3 state. However, strictly speaking, the Σ_3 state is dipole forbidden in this experimental geometry where the vector potential is perpendicular to the [001] direction. Therefore, this new state is an induced surface state due to increased

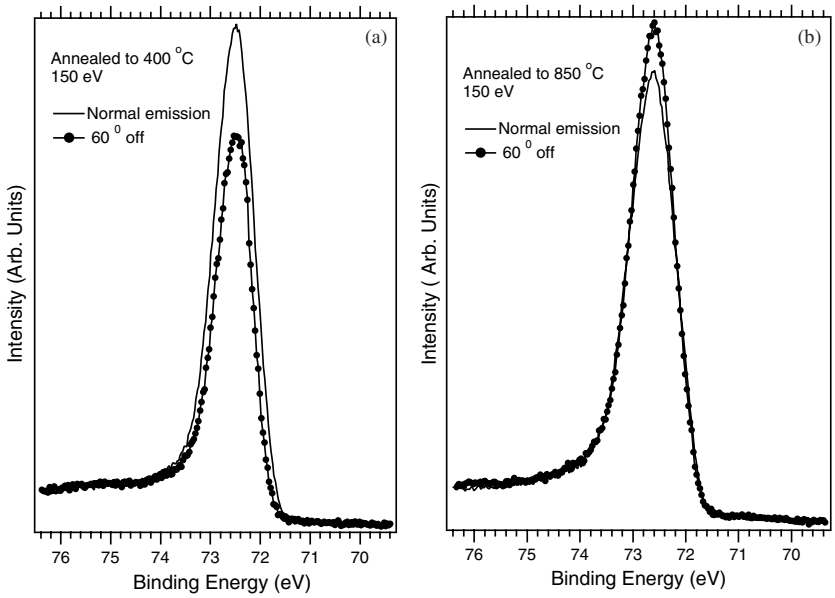

Figure 9. The Al 2p core level spectra taken in normal and 60° emission angle geometries (photon energy = 150 eV) for (a) bulk terminated and (b) incommensurate surfaces.

hybridization between Fe d band and Al sp bands resulting from the modified surface charge density. We presume that this state originates from the symmetry forbidden Σ_3 state admixed with the Al sp band. The impact of the hybridization on the Σ_3 state for the other symmetry direction, $\vec{A} \perp [001]$, is shown in figure 8, where a photon energy of 80 eV was employed. It is clear that the major differences between the two spectra are the reduced intensity for the Σ_1 state at 1.25 eV and an enhanced peak feature for the Σ_3 state at 0.6 eV, when the spectrum of the incommensurate surface is compared to that of the bulk terminated surface.

We also measured the shallow core level photoemission spectra of Al 2p and Fe 3p with normal and 60° emission angle geometries, at a photon energy of 150 eV, to corroborate the Al segregation occurring on the surface of FeAl(110). Figures 9(a) and (b) show the core level photoemission spectra of Al 2p taken at normal and 60° emission angles for bulk terminated and incommensurate surfaces, respectively. As the emission angle geometry is increased (i.e., from 0° to 60°), the integrated core level intensity becomes more surface sensitive due to the effective decrease in the probing depth. As shown in figure 9(a), the intensity of the Al 2p spectrum for the bulk terminated surface measured at normal emission is higher than that at the 60° emission angle. However, the opposite behaviour is observed for the incommensurate phase (figure 9(b)). The intensity of the Al 2p core level is relatively enhanced in the 60° emission angle geometry. Although not shown here, a lower intensity ratio of Al 2p to Fe 3p for the bulk terminated phase spectra compared to the incommensurate phase is also revealed. These results support the conclusion that Al atoms segregate to the surface region at elevated temperatures, as also supported by the STM measurements.

4. Conclusion

Surface segregation, which changes the surface/near surface composition structure, was found to be a fundamental feature in the atomic and the resultant electronic structure of the FeAl(110)

intermetallic alloy. Preferential sputtering results in a depleted Al surface and subsequent annealing promotes Al segregation to the near surface region. The segregation trend leads to new reconstructed phases. In contrast to previous AES and LEED studies, a bulk terminated surface is obtained after annealing the surface to 400 °C. An incommensurate phase occurs for annealing temperature above 800 °C. This phase is commensurate with the underlying substrate only along the $[1\bar{1}0]$ direction. The STM data reveal that this superstructure is composed of a quasi-hexagonal form of Fe atoms surrounded by six Al atoms. The AES and STM results are consistent with $FeAl_2$ stoichiometry for the topmost layer of FeAl(110). The ARPES measurements confirm the Al segregation with increased DOS near the Fermi level upon annealing the surface to 850 °C. The enhanced electronic state is assumed to be due to hybridization between the Fe d band and Al sp bands and is derived from the bulk Σ_3 state. The increased intensity of the Al 2p core level for the incommensurate phase with the higher emission angle also confirms the Al diffusion to the surface region.

Acknowledgments

We would like to acknowledge the staff of CAMD for their support in the photoemission studies. This work was sponsored in part by the US Department of Energy, under Contract No DE-AC05-00-OR22725 with the Oak Ridge National Laboratory, managed by UTBattelle, LLC. The research was also supported in part by US DOE contract No DE-FG02-98ER45712, NSF contract No ECS-0210583, and the Louisiana Board of Regents.

References

[1] Sauthoff G 1995 *Intermetallics* (Weinheim: VCH)
[2] Stoloff N S and Liu C T 1994 *Intermetallics* **2** 75
[3] Zou J and Fu C L 1995 *Phys. Rev.* B **51** 2115
[4] Davis H L and Noonan J R 1985 *Phys. Rev. Lett.* **54** 566
[5] Yalisove S M and Graham W R 1987 *Surf. Sci.* **183** 556
[6] Blum V, Rath C, Castro G R, Kottche M, Hammer L and Heinz K 1996 *Surf. Rev. Lett.* **3** 1409
[7] Graupner H, Hammer L, Müller K and Zehner D M 1995 *Surf. Sci.* **322** 103
[8] Hammer L, Graupner H, Blum V, Heinz K, Ownby G W and Zehner D M 1998 *Surf. Sci.* **412/413** 69
[9] Gleason N R and Strongin D R 1993 *Surf. Sci.* **295** 306
[10] Kizilkaya O, Hite D A, Zehner D M and Sprunger P T, unpublished
[11] Köster W and Gödecke T 1980 *Z. Metallk.* **71** 765
[12] Landolt–Börnstein 1991 Phase equilibria *Crystallographic and Thermodynamic Data of Binary Alloys* (Berlin: Springer)
[13] Kottcke M, Graupner H, Zehner D M, Hammer L and Heinz K 1996 *Phys. Rev.* B **54** R5275
[14] Meier W, Blum V, Hammer L and Heinz K 2001 *J. Phys.: Condens. Matter* **13** 1781
[15] Højrup Hansen K, Gottschalck J, Petersen L, Hammer B, Lægsgaard E, Besenbacher F and Stensgaard I 2001 *Phys. Rev.* B **63** 115421
[16] Baddorf A P and Chandavarkar S S 1996 *Physica* B **221** 141
[17] Kang M H and Mele E J 1987 *Phys. Rev.* B **36** 7371
[18] Das G P, Rao B K, Jena P and Deevi S C 2002 *Phys. Rev.* B **66** 184203